Article

Ligand-Based Design of Selective Peptidomimetic uPA and TMPRSS2 Inhibitors with Arg Bioisosteres

Patrick Müller [ID]**, Collin Zimmer** [ID]**, Ariane Frey, Gideon Holzmann, Annabelle Carolin Weldert** [ID]
and Tanja Schirmeister *

Institute of Pharmaceutical and Biomedical Sciences, Johannes Gutenberg University Mainz, Staudinger Weg 5,
D-55128 Mainz, Germany; muelpat@uni-mainz.de (P.M.); cozimmer@uni-mainz.de (C.Z.);
arfrey@uni-mainz.de (A.F.); gholzman@students.uni-mainz.de (G.H.); anwelder@uni-mainz.de (A.C.W.)
* Correspondence: schirmei@uni-mainz.de; Tel.: +49-6131-39-25742

Abstract: Trypsin-like serine proteases are involved in many important physiological processes like blood coagulation and remodeling of the extracellular matrix. On the other hand, they are also associated with pathological conditions. The urokinase-pwlasminogen activator (uPA), which is involved in tissue remodeling, can increase the metastatic behavior of various cancer types when overexpressed and dysregulated. Another member of this protease class that received attention during the SARS-CoV 2 pandemic is TMPRSS2. It is a transmembrane serine protease, which enables cell entry of the coronavirus by processing its spike protein. A variety of different inhibitors have been published against both proteases. However, the selectivity over other trypsin-like serine proteases remains a major challenge. In the current study, we replaced the arginine moiety at the P1 site of peptidomimetic inhibitors with different bioisosteres. Enzyme inhibition studies revealed that the phenylguanidine moiety in the P1 site led to strong affinity for TMPRSS2, whereas the cyclohexylguanidine derivate potently inhibited uPA. Both inhibitors exhibited high selectivity over other structurally similar and physiologically important proteases.

Keywords: trypsin-like serine proteases; covalent reversible inhibitors; enzyme inhibition study; protease inhibitors; peptidomimetic sequence; arginine bioisosteres

1. Introduction

With over 600 different proteins, proteases represent an important class of enzymes [1]. Approximately one-third of all known proteolytic enzymes are serine proteases [2]. According to the MEROPS database of peptidases, these enzymes are classified into clans by their catalytic mechanism and into families on the basis of a common ancestry [3]. The largest family of serine proteases are the trypsin-like proteases (TLPs). The catalytic triad of TLPs harbors a nucleophilic serine residue in combination with aspartate and histidine, which increase the nucleophilicity of the serine. The trypsin-like substrate specificity is characterized by the positively charged side chain of arginine or lysine in the P1 position [3,4]. Numerous important physiological processes rely on trypsin-like serine proteases. This includes hemostasis, the immune response system and extracellular matrix remodeling [5–8]. Dysregulation of these enzymes can lead to severe pathological incidents, which range from cardiovascular disorders to cancer progression or neurodegenerative and inflammation processes [8–10]. Moreover, proteases often are virulence factors in infectious diseases. As an example, tropical and subtropical countries are heavily affected by dengue virus infections, where the viral NS2B-NS3 trypsin-like serine protease is essential for the replication process of the virus [11]. Undoubtedly, this class of enzymes includes promising targets in various diseases, and the scientific community still strives to discover more drug candidates [7].

The urokinase-type plasminogen activator (uPA) is one member of the trypsin-like serine proteases. The enzyme is involved in the fibrinolytic system [12]. The binding of

uPA to its specific glycolipid-anchored uPA receptor (uPAR) on cell surfaces enables the conversion of plasminogen to the serine protease plasmin [13]. This mediates extracellular proteolysis and the activation of several further proteases, like activating growth factors and metalloproteases, which catalyze the degradation and remodeling of extracellular matrix components [14,15]. Unfortunately, pathophysiological mechanisms like tumor angiogenesis, tumor progression and metastasis profit from these events, and therefore, inhibition of this protease could be beneficial for the mitigation, or even prevention, of tumor proliferation (Figure 1 left side) [14,15]. Blocking of the catalytic activity was achieved by specific antibodies, overexpression of the endogenous inhibitors PAI-1 and small-molecule inhibitors [16–18]. One of the most promising peptidomimetic inhibitors, mesupron® (upamostat, WX-671, RHB-107, Wilex AG, Heidelberg, Germany), led to reduced metastasis and extended lifespan in clinical trials on pancreatic and breast cancer patients [19]. Hence, uPA can be considered as a promising drug target to block tumor dissemination.
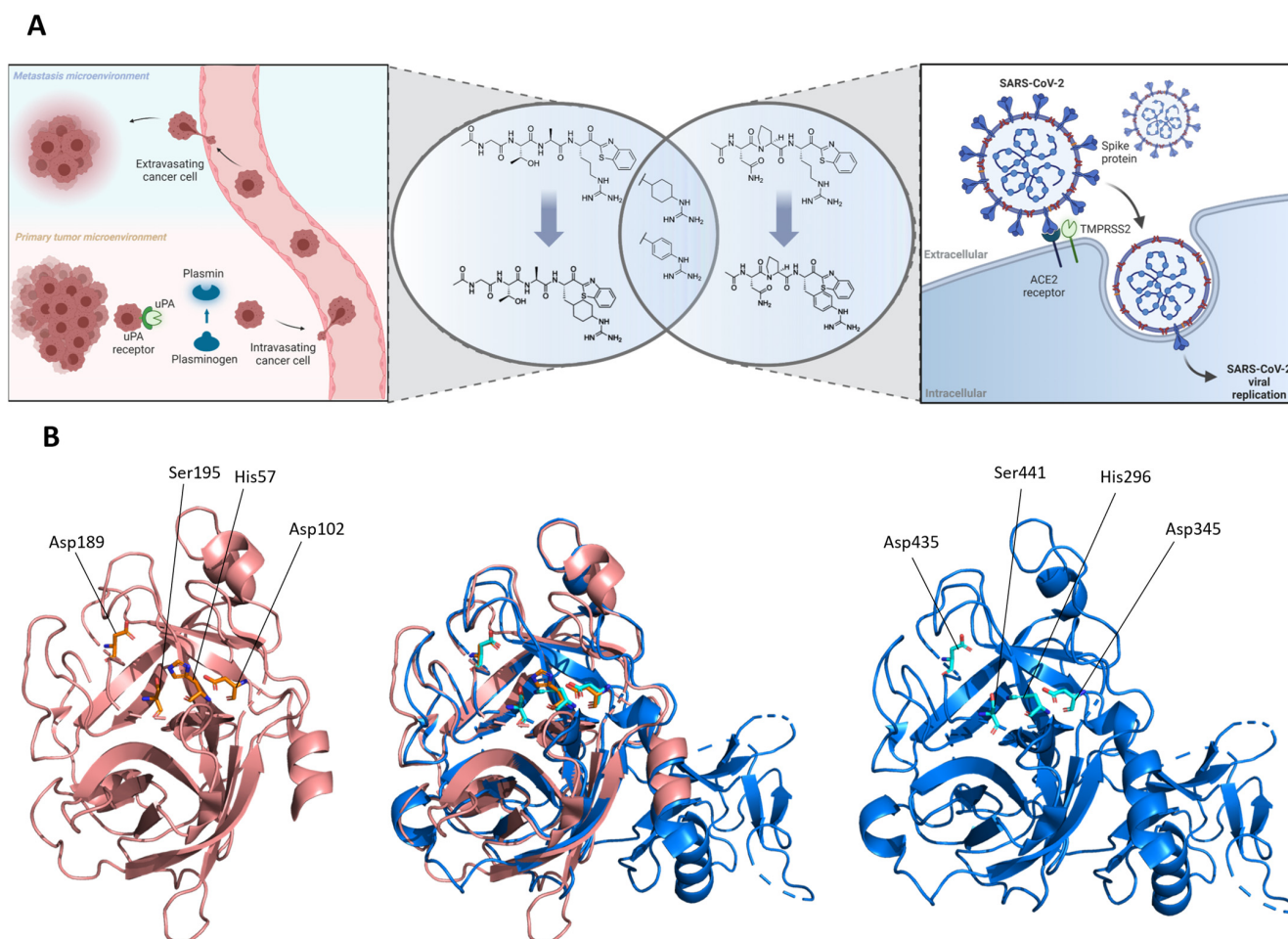

Figure 1. (**A**) Ligand-based design of covalent-reversible uPA (**left**) and TMPRSS2 (**right**) inhibitors with arginine bioisosteres. (**A**) Created with BioRender.com. (**B**) Visualization of the uPA structure (red, PDB: 7VM4) containing the catalytic triad (Asp102, His57, Ser195) and Asp189 in the S1 pocket, TMPRSS2 (blue, PDB: 7MEQ) containing the catalytic triad (Asp345, His296, Ser441) and Asp435 in the S1 pocket and the superimposition of both proteases (red/blue). (**B**) Created with PyMOL (Version 2.4.0, Schrödinger, LLC, New York, NY, USA).

Another proteolytic enzyme that belongs to the trypsin-like serine proteases is the human transmembrane protease serine subtype 2 (TMPRSS2). It has been shown to play an important role for viral host cell entry, and received increased attention during the SARS-CoV-2 pandemic due to its ability to enable cell entry and spread of the coronaviruses SARS-CoV-2, SARS-CoV and MERS-CoV [20–24]. The entry of these viruses is mediated by

the spike protein, which is located at the viral cell surface. TMPRSS2 processes the spike protein after binding of the virus to the angiotensin-converting enzyme 2 receptor (ACE2), initiating the entry into lung cells (Figure 1 right side) [23,25]. Additionally, viral cell entry can occur via the endosomal pathway, whereby the spike protein is processed by cathepsin L [26]. Studies have demonstrated that inhibition of TMPRSS2 blocks the viral host cell entry and replication of SARS-CoV-2 in lung epithelial Calu-3 cells [27,28]. Previous work, in cooperation with Mailänder et al. showed that peptidomimetic inhibitors efficiently reduce TMPRSS2 activity, block SARS-CoV-2 spike-driven entry and prevent SARS-CoV-2 infection in CaCo-2 cells [29]. This highlights the opportunity for an alternative therapeutic strategy, besides targeting of the viral host proteases papain-like protease (PL^{pro}) and the 3C-like- or "main protease" (3CL- or M^{pro}) [30–32].

In the past decades, several uPA inhibitors have been disclosed, most of them with non-covalent reversible or covalent-irreversible inhibition mode [16,33]. On the contrary, only few covalent-reversible inhibitors are found in the literature [34]. Such inhibitors could combine the benefits from both concepts: the high-affinity properties and extended residence time by covalent modification of the catalytic serine residue and the reduced risk for unwanted side effects and toxicity by a reversible binding mechanism [35–37]. Furthermore, in order to minimize the risk for side effects, it is of great importance to inhibit the target protease selectively. This, however, is a major challenge due to the high structural similarity within the trypsin-like serine protease family.

In 2021, the group around Huang et al. created a homology structure model of the TMPRSS2 serine protease domain, and revealed a high similarity between the homology model and the structure of the uPA [38]. This led to the idea to transfer the design of the synthesized uPA inhibitors to the previously published TMPRSS2 inhibitors, to receive an improved set of inhibitors in terms of off-target selectivity (Figure 1) [29].

Herein, we describe the ligand-based development of peptidomimetic inhibitors, which started with Ac-Gly-L-Thr-L-Ala-L-Arg-ketobenzothiazole (kbt) as a covalent-reversible uPA inhibitor discovered in previous work [39]. We substituted the P1-arginine moiety with a variety of bioisosteres, inspired by the serine protease inhibitor camostat, and furthermore modified the benzothiazole structure [40,41]. The cyclohexyl-and phenylguanidine moiety presented the most promising results during the enzyme inhibition studies. Therefore, we translated this structure motif to the suitable peptide sequence Ac-L-Asn-L-Pro-L-Arg-kbt from our previous work towards TMPRSS2 [29]. Within this study, we successfully enhanced the affinity and selectivity for both main-target proteases by systematic variation of different structural elements.

2. Results

2.1. Chemistry

All tested peptidomimetic inhibitors were synthesized in multistep reactions. First, the peptide sequences (P2–P4) of the inhibitors were prepared via a standard fmoc solid phase peptide synthesis (SPPS) protocol, which is described in detail in the Supporting Information. The P1 derivatives with the ketobenzothiazole moiety as warhead were prepared as described in Schemes 1 and 2.

2.1.1. Synthesis of the (Homo)arginine-Based Inhibitors

Boc-protected N_ω-2,2,4,6,7-pentamethyl-dihydrobenzofuran-5-sulfonyl (pbf)-L-arginine **4**, which was used as the starting material for the arginine-based inhibitors **14a–f** and **15**, was modified to the Weinreb amide **5**. The ketobenzothiazole derivatives **12a–f** and **13** were obtained by alkylation of **5** with the respective heterocycles **10a–f** and **11**. The benzothiazole **10a** and the benzothiophene **10f** were commercially available, whereas the 6-fluoro-, 6-chloro-, 6-bromo-, 6-methoxybenzothiazoles **10b–e** and 4,5,6,7-tetrahydrothiazole **11** had to be synthesized by desamination of the commercially available 2-amino precursors **6b–e** and **9**. The 2-amino-4,5,6,7-tetrahydrothiazole **9** was prepared from cyclohexane **7** and thiourea **8** with iodine. The preparation of the homoarginine inhibitor **20** started with

the guanylation of boc-protected L-lysine **16** with *N,N′*-bis-(carbobenzoxy)-1-*H*-pyrazole-1-carboxamidine, yielding compound **17**. Afterwards, **17** was converted to the ketobenzothiazole **19**, in analogy to the arginine derivatives. After boc-deprotection of the amino group, the P1 precursor derivatives were coupled with the Ac-Gly-L-Thr(O*t*Bu)-L-Ala-OH peptide **3** using 1-[bis(dimethylamino)methylene]-1*H*-1,2,3-triazolo [4,5-b]pyridinium 3-oxide hexafluorophosphate (HATU) as the coupling reagent. Final deprotection of the (homo)arginine and threonine side chain under acidic conditions and purification via RP-HPLC yielded the inhibitors **14a–f**, **15** and **20**.
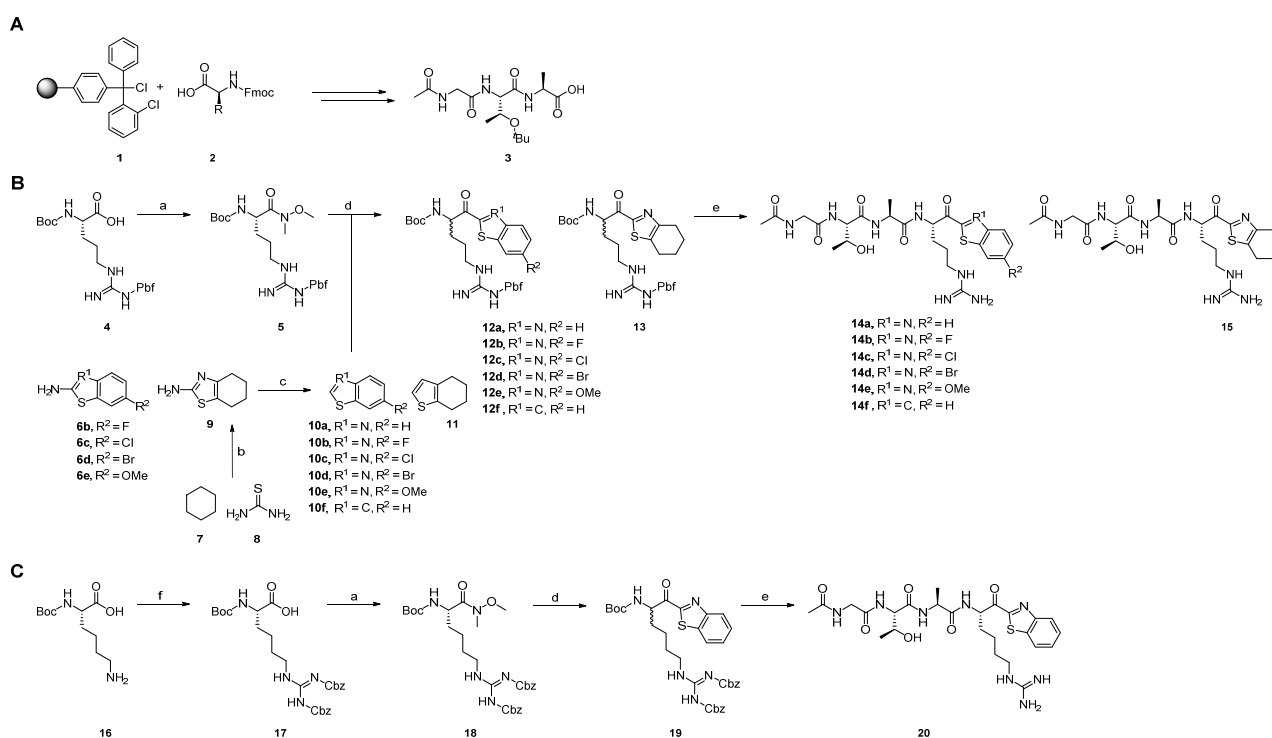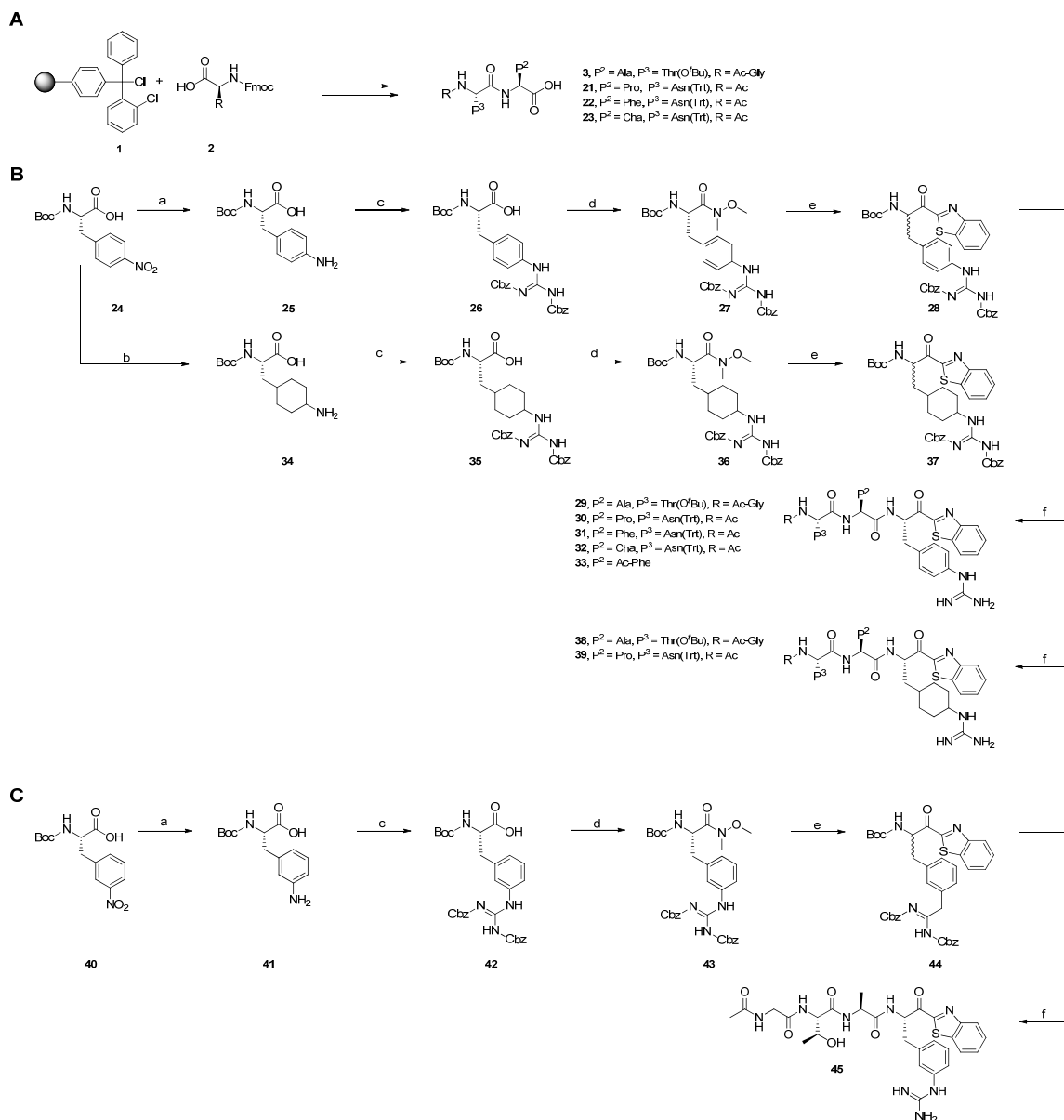

Scheme 1. Synthesis of the (homo)arginine-based inhibitors **14a–f**, **15**, **20**. (**A**) Solid phase peptide synthesis of peptide sequence **3**. (**B**) Preparation of the final arginine compounds **14a–f**, **15**. (**C**) Synthesis of the homoarginine inhibitor **20**. Reaction conditions: (a) *N,O*-dimethylhydroxylamine·HCl, TBTU, DIEA, DCM, rt, 12 h, 70–90%; (b) cyclohexane, thiourea, iodine, 130 °C, 12 h, 53%; (c) isopentyl nitrite, THF, reflux, 2–5 h, 46–76%; (d) benzothiazole-derivative, *n*-BuLi, THF, −78 °C, 2 h, 50–88%; (e) 1. TFA, DCM, rt, 0.5 h, 2. HATU, DIEA, DMF, DCM, rt, 12 h, 3. TFA, DCM, rt, 2 h, 4–10%; (f) *N,N′* bis-(carbobenzoxy)-1-*H*-pyrazole-1-carboxamidine, Et₃N, DMF, rt, 72 h, quant.

2.1.2. Synthesis of the Phenyl/Cyclohexylguanidine-Based Inhibitors

The preparation of the *p*-phenyl- and *p*-cyclohexylguanidine-based inhibitors both started with boc-protected *p*-nitro-L-phenylalanine **24**. The reduction of the nitro group was carried out with 5% Pd/C in methanol to yield **25**, whereas the hydrogenation of the benzene ring and the nitro group using the Adam's catalyst under acidic conditions yielded the cyclohexane derivative **34**. The amine group of both compounds was guanylated with *N,N′*-cbz-(carbobenzoxy)-1-*H*-pyrazole-1-carboxamidine. The bis-cbz-protected intermediates (**26**, **35**) were converted, in a similar way to the arginine-based inhibitors (Section 2.1.1), to the Weinreb amides **27** and **36** and later to the ketobenzothiazole derivatives **28** and **37**. After removal of the boc-protecting groups, the respective peptide sequences **3**, **21–23**, which were synthesized via a standard fmoc solid-phase synthesis (SPPS), were coupled with the *p*-phenyl- and cyclohexylguanidine precursor derivatives. After final deprotection of the side chains in TFA/DCM and purification via RP-HPLC, the inhibitors **29–33** and **38–39** were obtained. Starting with *m*-nitro-L-phenylalanine **40**, the inhibitor **45** was prepared in analogy to the 5-step synthetic process of the *p*-phenylguanidine derivatives **29–33**.

The synthesized final compounds **14a–f**, **15**, **20**, **29–33**, **38–39**, **45** showed two peaks with identical m/z ratio and similar retention times in initial chromatographic analyses. This is due to the partial epimerization of the α-carbon in the P1 amino acid portion during the reaction of the Weinreb amide with lithium-benzothiazole solution. Since the faster eluting epimer was always isolated via RP-HPLC in very large excess, while the other diastereomer was obtained only in traces, we supposed the first one to be the L-epimer, and used it for all inhibition studies [42].

Scheme 2. Synthesis of the phenyl/cyclohexylguanidine-based inhibitors **29–33**, **38–41**, **45**. (**A**) Solid phase peptide synthesis of peptide sequences **3**, **21–23**. (**B**) Preparation of the final *p*-phenyl/cyclohexylguanidine compounds **29–33**, **38–41**. (**C**) Synthesis of the *m*-phenylguanidine inhibitor **45**. Reaction conditions: (a) 1. Pd/C 5%, H$_2$ (3 bar), MeOH, 3 h, (b) PtO$_2$, H$_2$ (3 bar), AcOH, MeOH, rt, 24 h, (c) *N,N'*-bis-(carbobenzoxy)-1-*H*-pyrazole-1-carboxamidine, Et$_3$N, DMF, rt, 6 h, 90%–quant.; (d) *N,O*-dimethylhydroxylamine·HCl, TBTU, DIEA, DCM, rt, 12 h, 51–53%; (e) benzothiazole, *n*-BuLi, THF, −78 °C, 2 h, 64–84%, (f) 1. TFA, DCM, rt, 0.5 h, 2. HATU, DIEA, DMF, DCM, rt, 12 h, 3. TFA, DCM, rt, 2 h, 10–40%.

2.2. Enzyme Inhibition Studies

The inhibitory activity of the synthesized compounds towards the respective main- and off-target proteases was measured via fluorometric and colorimetric assays. Thus, fluorogenic AMC- or colorimetric *p*NA-based substrates with a peptide sequence suitable for the tested protease were utilized (see Supplementary Figure S2). At first, the compounds were screened against five proteases (uPA, TMPRSS2, matriptase, tPA, thrombin, factor Xa) at 20 μM, and a cut-off value of 80% inhibition at this concentration was set, for the differentiation between nonactive (n.a.) and active inhibitors. Due to the reversible inhibition mechanism of the ketobenzothiazole derivates, the IC_{50} values were determined with Graphpad Prism 9, and afterwards converted to the corresponding K_i values for an adequate comparison between the inhibitory activities of the compounds toward all tested proteases. The K_i values were calculated using the Cheng–Prusoff equation [43].

2.2.1. Inhibition Studies with uPA Inhibitors

At first, we investigated the selectivity profile of the starting compound **14a,** which exhibited good inhibition of uPA with a K_i value of 141 nM. **14a** was originally synthesized for the analysis of reactivity and selectivity studies of peptidomimetic covalent inhibitors [40]. The peptide sequence Ac-L-Gly-L-Thr-L-Ala-L-Arg was used, because of its literature-known selectivity for uPA vs. tPA [44]. Due to the similar and important physiological roles of uPA and tPA, a good selectivity is necessary to avoid severe side effects concerning ECM degradation and cell proliferation [5,45,46]. Furthermore, the trypsin-like serine proteases thrombin and factor Xa were chosen because of their important roles in blood coagulation, as well as matriptase as a representative of a transmembrane protease, which is involved in the remodeling of plasma membranes and other lipid matrix formations [47–49]. Due to their structural similarity (calculated sequence similarity is given in Tables 1–3) to uPA and their physiological roles, they resemble important off-targets. As expected, **14a** did not show inhibition of tPA, and only moderate selectivities for uPA towards thrombin (**14a** K_i = 4390 nM) and factor Xa (**14a** K_i = 3360 nM) with inhibition constants in the low micromolar range. In contrast, a lower K_i value was obtained for mapriptase (**14a** K_i = 32 nM). Exchanging the arginine side chain with a *p*-phenyl- or cyclohexylguanidine moiety enhanced the inhibitory properties. Both derivates resulted in more affine inhibitors (**29** K_i = 29 nM, **38** K_i = 39 nM), with a significant improvement in their selectivity profiles. The inhibitors **29**, **38** did not inhibit tPA, thrombin and factor Xa, and the selectivity indices for matriptase (**29** K_i = 132 nM, **38** K_i = 626 nM) were improved. The inhibitors **20** and **45**, which contain the homoarginine and *m*-substituted phenylguanidine moiety, did not show inhibition of all tested proteases at 20 μM, which highlights the importance of the alkyl chain length and the *p*-position of the guanidine element for proper binding into the S1 pocket. Additionally, all compounds were tested against the TMPRSS2 because of the aforementioned structure similarity to uPA [38]. The results indicated a strong affinity to the TMPRSS2 protease with K_i values in the nanomolar range of the arginine, phenyl- and cyclohexyl derivates (**14a** K_i = 5 nM, **29** K_i = 10 nM, **38** K_i = 73 nM). Based on these results, a SAR study with the phenyl- and cyclohexylguanidine moiety as arginine bioisosteres for new TMPRSS2 inhibitors was performed, which is described in Section 2.2.2 [29].
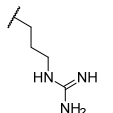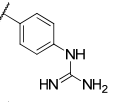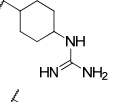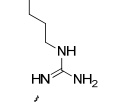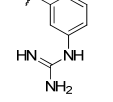
Besides the arginine replacement in the P1 position, we also evaluated the influence of modifications of the benzothiazole moiety (cpds. **14b–f, 15**). The introduction of the electronegative halogen atoms fluorine, chlorine and bromine in position 6 led to an approximately two-fold increase in the affinity for the chloro- and bromo-derivates (**14c** K_i = 82 nM, **14d** K_i = 60 nM), and a three-fold loss of affinity for the fluoro-derivate (**14b** K_i = 388 nM). Other modifications, like the electron-donating methoxy group in position 6 (**14e** K_i = 178 nM), the exchange of the benzene ring system with a cyclohexyl ring (**15** K_i = 435 nM) or the replacement of the benzothiazole with a benzothiophene ring, led to a decrease in or complete loss of the affinity towards the uPA. Selectivity studies were performed with the chloro- and bromo-derivates **14c–d**, because they were

the only inhibitors with slightly better affinity than the nonsubstituted ketobenzothiazole inhibitor **14a**. They revealed similar affinity to TMPRSS2 (**14c** K_i = 9 nM, **14d** K_i = 6 nM) and matriptase (**14c** K_i = 59 nM, **14d** K_i = 38 nM), and reduced selectivity vs. thrombin (**14c** K_i = 456 nM, **14d** K_i = 450 nM) and factor Xa (**14c** K_i = 2447 nM, **14d** K_i = 2847 nM) in comparison to **14a**.

Table 1. Inhibition data (K_i values and selectivity indices [SI]) of the synthesized uPA inhibitors **14a**, **20**, **29**, **38**, **45** towards uPA, TMPRSS2, matriptase, tPA, thrombin and factor Xa.
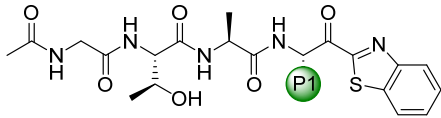
14a, 20, 29, 38, 45

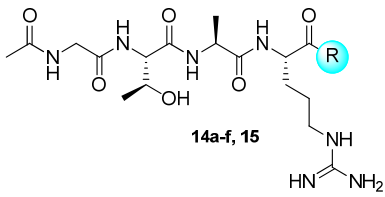| Compound		K_i [nM] [SI]					
P1		uPA	TMPRSS2 55.6%	Matriptase 68.9%	tPA 66.7	Thrombin 60.0%	Factor Xa 62.2%
	14a	141 ± 28	5 ± 1 [0.04]	32 ± 14 [0.2]	n.a.	4390 ± 1480 [31]	3360 ± 320 [24]
	29	29 ± 2	10 ± 4 [0.3]	133 ± 3 [4]	n.a.	n.a.	n.a.
	38	39 ± 5	73 ± 16 [1.8]	626 ± 74 [16]	n.a.	n.a.	n.a.
	20	n.a.	n.a.	n.a.	n.a.	n.a.	n.a.
	45	n.a.	n.a.	n.a.	n.a.	n.a.	n.a.

Selectivity indices [SI] represent the quotient of the K_i values for TMPRSS2, matriptase, tPA, thrombin and factor Xa to the K_i value for uPA; n.a. not active, i.e., <80% inhibition at 20 µM; calculated sequence similarity between the binding sites of uPA and the other proteases are given in %.

2.2.2. Inhibition Studies with TMPRSS2 Inhibitors

The selection of the peptide sequence Ac-L-Asn-L-Pro-L-Arg was based on the results of previous work. The published inhibitor Ac-L-Asn-L-Pro-L-Arg-kbt showed K_i values in the single-digit nanomolar range (K_i = 2.5 nM) and a good selectivity vs. thrombin (K_i = 1046 nM) [29]. Unfortunately, only slight selectivity could be observed over factor Xa (K_i = 41.1 nM), and almost no difference in inhibition potency between TMPRSS2 and matriptase (K_i = 5.2 nM). Therefore, we tried to improve the selectivity profile by substituting the arginine side chain in the P1 position with the previously used phenyl- and cyclohexylguanidine moiety. Both derivates **30**, **39** showed an increase in selectivity for TMPRSS2 towards matriptase, with the phenylguanidine-based compound being more affine for TMPRSS2 (**30** K_i = 5 nM) than the cyclohexyl derivate (**39** K_i = 44 nM), but also showing a better inhibition of the matriptase for the phenylguanidine derivate (**30** K_i = 60 nM, **39** K_i = 1198 nM). **30**–**33** and **39** did not inhibit tPA, thrombin and factor Xa. In addition, **30** and **39** showed a moderate selectivity for TMPRSS2 over uPA (**30** K_i = 479 nM, **39** K_i = 936 nM). Based on these results, and due to the overall good affinity and selectivity parameters, we decided to maintain the phenylguanidine moiety in the P1 position and implement P2 modifications with phenyl- and cyclohexylalanine (Phe, Cha) instead of proline. The latter is based on results obtained with hepsin inhibitors from the group of

Kwon et al. [40]. The inhibitor **31** with the P2 phenylalanine residue showed inhibition of TMPRSS2 in the subnanomolar range (**31** K_i = 0.4 nM) and a significant increase in selectivity over matriptase (**31** K_i = 252 nM) and uPA (**31** K_i = 3574 nM). The inhibitor **32** with the cyclohexylalanine residue in P2 position also showed very good selectivity over matriptase (**32** K_i = 3333 nM) and uPA (**32** K_i = 2688 nM), but less affinity to TMPRSS2 (**32** K_i = 34 nM). In an attempt to improve the drug-like properties of the designed inhibitors, we synthesized the shortened compound **33**. This led to a slightly less active TMPRSS2 inhibitor, but still in the low nanomolar range (**33** K_i = 5 nM). The selectivity profile for TMPRSS2 inhibition over matriptase (**33** K_i = 1443 nM) and uPA (**33** K_i = 5264 nM) is still very promising.

Table 2. Inhibition data (K_i values and selectivity indices [SI]) of the synthesized uPA inhibitors **14a–f**, **15** towards uPA, TMPRSS2, matriptase, tPA, thrombin and factor Xa.

Compound		K_i [nM] [SI]					
R		uPA	TMPRSS2 55.6%	Matriptase 68.9%	tPA 66.7	Thrombin 60.0%	Factor Xa 62.2%
(benzothiazole)	**14a**	141 ± 28	5 ± 1 [0.04]	32 ± 14 [0.2]	n.a.	4390 ± 1480 [31]	3360 ± 320 [23]
(benzothiazole-F)	**14b**	388 ± 95	-	-	-	-	-
(benzothiazole-Cl)	**14c**	82 ± 6	9 ± 1 [0.1]	59 ± 9 [0.7]	n.a.	456 ± 72 [5]	2447 ± 99 [30]
(benzothiazole-Br)	**14d**	60 ± 15	6 ± 1 [0.1]	38 ± 2 [0.6]	n.a.	450 ± 69 [8]	2847 ± 844 [47]
(benzothiazole-OMe)	**14e**	178 ± 19	-	-	-	-	-
(benzothiophene)	**14f**	n.a.	-	-	-	-	-
(tetrahydrobenzothiazole)	**15**	435 ± 33	-	-	-	-	-

Selectivity indices [SI] represent the quotient of the K_i values for TMPRSS2, matriptase, tPA, thrombin and factor Xa to the K_i value for uPA; n.a., not active, i.e., <80% inhibition at 20 µM; "-", not tested; calculated sequence similarity between the binding sites of uPA and the other proteases are given in %.

2.3. Parallel Artificial Membrane Permeation Assay (PAMPA)

Following the envisioned applications of the presented inhibitors as drug leads for the treatment of cancer or viral infections, cell permeability is an important factor in the characterization process. Since both main targets (uPA and TMPRSS2) are membrane-located, extracellular structures, inhibitors seemingly do not require cell permeation to address their target. However, in the organismic contexts of oral bioavailability (facilitated application) and biodistribution (reaching target tissue), adequate permeation is an important quality. To assess this characteristic, PAMPA was used as a suitable model for passive permeation.

Generally, the inhibitor scaffold combines some favorable features: The Arg-like P1 amino acid (in combination with other hydrophilic amino acids like Asp and Thr)

ensures high aqueous solubility, even in the presence of the rather hydrophobic benzo-heteroarenes. The latter motif conveys reliable detectability by spectroscopy-based methods (λ_{max} = 305–350 nm, depending on substitution pattern). The inhibitors also were found to be sufficiently stable in the utilized aqueous system (50 mM TRIS, pH = 7.4) over the course of the assay (7 h at room temperature) and under elevated temperature conditions (17 h at 37 °C). Computed physicochemical properties, absorption spectra and stability studies are depicted in Supplementary Figures S4 and S5 and Table S1.

Table 3. Inhibition data (K_i values and selectivity indices [SI]) of the synthesized TMPRSS2 inhibitors **30–33**, **39** towards TMPRSS2, uPA, matriptase, tPA, thrombin and factor Xa.

30-33, 39
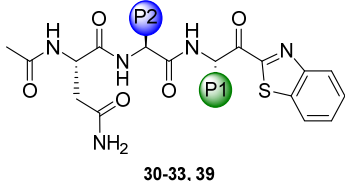
Compound			K_i [nM] [SI]					
P2	P1		TMPRSS2	uPA 53.2%	Matriptase 66.7%	tPA 62.2%	Thrombin 57.8%	Factor Xa 66.7%
Pro	Arg [31]		2.5	-	5.2 [2]	-	1046 [418]	41.1 [16]
Pro		**30**	5 ± 1	479 ± 17 [96]	60 ± 8 [12]	n.a.	n.a.	n.a.
Pro		**39**	44 ± 7	936 ± 100 [21]	1198 ± 181 [27]	n.a.	n.a.	n.a.
Phe		**31**	0.4 ± 0.1	3574 ± 421 [>5000]	252 ± 67 [630]	n.a.	n.a.	n.a.
Cha		**32**	34 ± 4	2688 ± 217 [79]	3333 ± 1141 [98]	n.a.	n.a.	n.a.
		33	5 ± 2	5264 ± 922 [1052]	1443 ± 90 [289]	n.a.	n.a.	n.a.

Selectivity indices [SI] represent the quotient of the K_i values for uPA, matriptase, tPA, thrombin and factor Xa to the K_i value for TMPRSS2; n.a., not active, i.e., <80% inhibition at 20 µM; "-", not tested; calculated sequence similarity between the binding sites of TMPRSS2 and the other proteases are given in %.

However, all presented compounds were found to have very low permeabilities (P_e < 1 × 10^{-6} cm/s) without any indication of improvement between the structural modifications (as exemplified for **38** in Figure 2). This result is not surprising. The pK_a (of the protonated guanidine function) of all compounds is calculated to be ≥10 (Marvin JS 23.11.0), meaning that in assay (or physiologic) conditions, all compounds are expected to be fully (≥99.75%) protonated, and therefore remarkably hydrophilic. Most of the presented compounds have negative logD$_{7.4}$ values, with **33** being the exception (logD$_{7.4}$ = 1.2; compare Supplementary Table S1). This level of lipophilicity, however, was still not enough to exert measurable permeability. For approved drugs with similar structural characteristics (e.g., camostat, melagatran, xylometazoline, metformin), only very limited permeabilities are described as well [50–53]. All this indicates the pronounced hindering effect of the guanidine group for passive permeation.

The discussed properties of the presented compounds can be paralleled to BCS class III compounds, namely their high aqueous solubility and low permeability. For these types of drugs, one major option to improve permeability is to remove charge from the molecule. In amidine-containing drugs, where charge is almost pH-independent due to their immense basicity, this was addressed by conversion to the amidoxime (ximelagatran or mesupron®) or carbamate prodrugs (dabigatran) with lower basicities [19,50,54]. For the guanidine moiety, the conversion to *N*-hydroxyguanidine is possible [55]. In a technological approach

to improved absorption, possible options for oral application are the formulation with permeation enhancing agents, or lipophilic counter ions [56]. For intravenous applications, nanoparticular formulations can be applied (e.g., for doxorubicin or for protease inhibitors) [57,58]. Of course, combinations of both chemical and technological approaches should be employed for optimization.
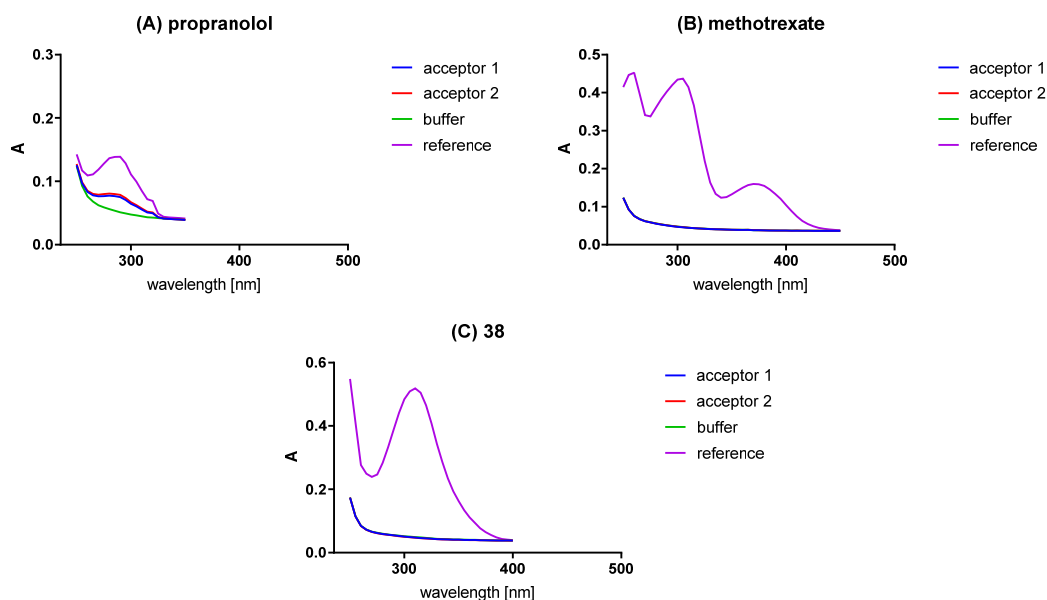

Figure 2. (**A**) Analysis of PAMPA permeable control propranolol HCl. (**B**) Analysis of PAMPA impermeable control methotrexate. (**C**) Analysis of PAMPA for **38**, representative of all synthesized final compounds of this study. All absorption spectra were baseline-corrected with the measured buffer spectrum at $\lambda \geq 450$ nm prior to AUC calculations. The reference spectra represent manually prepared samples, equivalent to a maximally permeated experimental sample. The acceptor spectra result from membrane permeation experiments and their AUC are proportional to the concentration of permeated compound.

3. Discussion

Trypsin-like serine proteases present attractive drug targets for treatment against many diseases, which can be of malignant cellular or viral origin [9,11]. Over the past decades many potent inhibitors were designed with remarkable affinity for the target protease. But most of them lack selectivity because of the highly structural similarity between the proteases. Within our study, we describe a systematic ligand-based approach to enhance affinities and selectivities. Starting from the previous published covalent reversible ketobenzothiazole inhibitor Ac-Gly-L-Thr-L-Ala-L-Arg-kbt **14a**, we modified the P1 arginine side chain with different bioisosteres [39]. The results indicate that the cyclohexylguanidine moiety fits best for uPA inhibition. The inhibitor **38** showed remarkable inhibition with a K_i value of 39 nM and a very good selectivity profile towards the other trypsin-like serine proteases. The modification of the benzothiazole moiety did not improve either the inhibitory properties nor the selectivity profiles, rendering the original kbt warhead the most promising.

The transfer of the P1-arginine replacement with the promising phenyl- and cyclohexylguanidine moieties to the previously published TMPRSS2 inhibitor Ac-L-Asn-L-Pro-L-Arg-kbt was a success, leading to a subnanomolar TMPRSS2 inhibitor **31** ($K_i = 0.4$ nM), with significantly increased selectivity over other trypsin-like serine proteases [29]. Furthermore, the shortened peptide sequence of the TMPRSS2 inhibitor **31** led to the more drug-like candidate **33,** with still very good inhibitory and selectivity properties. In terms of permeability, the inhibitor scaffold (and especially the shortened compound **33**) leaves the opportunity for improvement in a focused structure-permeability relationship study.

4. Materials and Methods

The materials as well as the methods used for this study are described in the Supporting Information. The authors have cited additional references within the Supporting Information [29,39,40,43,59–72]. Supplementary Figures of the protein similarity calculation (Figure S1), fluorometric inhibition assays (Figures S2 and S3), absorption spectra (Figure S4), stability studies (Figure S5), NMR-spectra and HPLC-chromatograms (Figures S6a–S21c) and Table S1 of the computation of physicochemical parameters can be accessed in the supporting information.

Abbreviations

Ac	acetyl
Ac-Gly	acetylglycine
AcOH	acetic acid
Ala	alanine
AMC	7-amino-4-methyl coumarine
Asn	asparagine
Boc:	*t*-butyloxy carbonyl
Cbz	benzyloxycarbonyl
Cha	cyclohexylalanine
DCM	dichloromethane
DIEA	*N,N*-diisopropylethylamine
DMSO	dimethylsulfoxide
Et$_3$N	triethylamine
Fmoc	9-Fluorenylmethoxycarbonyl
h	hours
HATU	2-(7-azabenzotriazol-1-yl)-*N,N,N′,N′*-tetramethyluronium hexafluorophosphate
MeOH	methanol
MERS-CoV	Middle East Respiratory Syndrome
n-BuLi	*n*-butyllithium
O^{t}Bu	*O-tert*-butyl
Pbf	N_ω-2,2,4,6,7-pentamethyl-dihydrobenzofuran-5-sulfonyl
Phe	phenylalanine
*p*NA	*para*-nitroanilide
Pro	proline
quant	quantitative
RP-HPLC	reversed phase high pressure liquid chromatography

rt	room temperature
SARS-CoV-2	severe acute respiratory syndrome coronavirus type 2
SPPS	solid phase peptide synthesis
TA	thioanisole
TBTU	2-(1*H*-Benzotriazole-1-yl)-1,1,3,3-tetramethylaminium tetrafluoroborate
TFA	trifluoroacetic acid
THF	tetrahydrofurane
TLP	trypsin-like serine protease
TMPRSS2	transmembrane protease serine subtype 2
tPA	tissue-type plasminogen activator
trt	triphenylmethyl
uPA	urokinase-type plasminogen activator
uPAR	urokinase-type plasminogen activator receptor

References

1. López-Otín, C.; Overall, C.M. Protease degradomics: A new challenge for proteomics. *Nat. Rev. Mol. Cell Biol.* **2002**, *3*, 509–519. [CrossRef] [PubMed]
2. Di Cera, E. Serine proteases. *IUBMB Life* **2009**, *61*, 510–515. [CrossRef] [PubMed]
3. Rawlings, N.D.; Morton, F.R.; Kok, C.Y.; Kong, J.; Barrett, A.J. MEROPS: The peptidase database. *Nucleic Acids Res.* **2007**, *36*, 320–325. [CrossRef] [PubMed]
4. Ma, W.; Tang, C.; Lai, L. Specificity of Trypsin and Chymotrypsin: Loop-Motion-Controlled Dynamic Correlation as a Determinant. *Biophys. J.* **2005**, *89*, 1183–1193. [CrossRef] [PubMed]
5. Lu, P.; Takai, K.; Weaver, V.M.; Werb, Z. Extracellular Matrix Degradation and Remodeling in Development and Disease. *Cold Spring Harb. Perspect. Biol.* **2011**, *3*, a005058. [CrossRef]
6. Oncul, S.; Afshar-Kharghan, V. The interaction between the complement system and hemostatic factors. *Curr. Opin. Hematol.* **2020**, *27*, 341–352. [CrossRef]
7. Ferguson, T.E.G.G.; Reihill, J.A.; Martin, S.L.; Walker, B. Novel Inhibitors and Activity-Based Probes Targeting Trypsin-Like Serine Proteases. *Front. Chem.* **2022**, *10*, 782608. [CrossRef]
8. Yaron, J.R.; Zhang, L.; Guo, Q.; Haydel, S.E.; Lucas, A.R. Fibrinolytic Serine Proteases, Therapeutic Serpins and Inflammation: Fire Dancers and Firestorms. *Front. Cardiovasc. Med.* **2021**, *8*, 648947. [CrossRef]
9. Eatemadi, A.; Aiyelabegan, H.T.; Negahdari, B.; Mazlomi, M.A.; Daraee, H.; Daraee, N.; Eatemadi, R.; Sadroddiny, E. Role of protease and protease inhibitors in cancer pathogenesis and treatment. *Biomed. Pharmacother.* **2017**, *86*, 221–231. [CrossRef]
10. Wu, Q.; Kuo, H.-C.; Deng, G.G. Serine proteases and cardiac function. *Biochim. Biophys. Acta-Proteins Proteom.* **2005**, *1751*, 82–94. [CrossRef]
11. Nitsche, C.; Holloway, S.; Schirmeister, T.; Klein, C.D. Biochemistry and Medicinal Chemistry of the Dengue Virus Protease. *Chem. Rev.* **2014**, *114*, 11348–11381. [CrossRef] [PubMed]
12. Dreymann, N.; Wuensche, J.; Sabrowski, W.; Moeller, A.; Czepluch, D.; Van, D.V.; Fuessel, S.; Menger, M.M. Inhibition of Human Urokinase-Type Plasminogen Activator (uPA) Enzyme Activity and Receptor Binding by DNA Aptamers as Potential Therapeutics through Binding to the Different Forms of uPA. *Int. J. Mol. Sci.* **2022**, *23*, 4890–4912. [CrossRef] [PubMed]
13. Mahmood, N.; Mihalcioiu, C.; Rabbani, S.A. Multifaceted Role of the Urokinase-Type Plasminogen Activator (uPA) and Its Receptor (uPAR): Diagnostic, Prognostic, and Therapeutic Applications. *Front. Oncol.* **2018**, *8*, 24. [CrossRef] [PubMed]
14. Mekkawy, A.H.; Pourgholami, M.H.; Morris, D.L. Involvement of Urokinase-Type Plasminogen Activator System in Cancer: An Overview. *Med. Res. Rev.* **2014**, *34*, 918–956. [CrossRef] [PubMed]
15. Masucci, M.T.; Minopoli, M.; Di Carluccio, G.; Motti, M.L.; Carriero, M.V. Therapeutic Strategies Targeting Urokinase and Its Receptor in Cancer. *Cancers* **2022**, *14*, 498. [CrossRef] [PubMed]
16. Buckley, B.J.; Aboelela, A.; Minaei, E.; Jiang, L.X.; Xu, Z.; Ali, U.; Fildes, K.; Cheung, C.-Y.; Cook, S.M.; Johnson, D.C.; et al. 6-Substituted Hexamethylene Amiloride (HMA) Derivatives as Potent and Selective Inhibitors of the Human Urokinase Plasminogen Activator for Use in Cancer. *J. Med. Chem.* **2018**, *61*, 8299–8320. [CrossRef] [PubMed]
17. Ma, D.; Gerard, R.D.; Li, X.-Y.; Alizadeh, H.; Niederkorn, J.Y. Inhibition of Metastasis of Intraocular Melanomas by Adenovirus-Mediated Gene Transfer of Plasminogen Activator Inhibitor Type 1 (PAI-1) in an Athymic Mouse Model. *Blood* **1997**, *90*, 2738–2746. [CrossRef] [PubMed]
18. Ossowski, L.; Russo-Payne, H.; Wilson, L.E. Inhibition of Urokinase-type Plasminogen Activator by Antibodies: The Effect on Dissemination of a Human Tumor in the Nude Mouse. *Cancer Res.* **1991**, *51*, 274–281.
19. Schmitt, M.; Harbeck, N.; Brünner, N.; Jänicke, F.; Meisner, C.; Mühlenweg, B.; Jansen, H.; Dorn, J.; Nitz, U.; Kantelhardt, E.J.; et al. Cancer therapy trials employing level-of-evidence-1 disease forecast cancer biomarkers uPA and its inhibitor PAI-1. *Expert Rev. Mol. Diagn.* **2011**, *11*, 617–634. [CrossRef]
20. Leow, M.K.-S. Correlating Cell Line Studies With Tissue Distribution of DPP4/TMPRSS2 and Human Biological Samples May Better Define the Viral Tropism of MERS-CoV. *J. Infect. Dis.* **2013**, *208*, 1350–1351. [CrossRef]

21. Bertram, S.; Heurich, A.; Lavender, H.; Gierer, S.; Danisch, S.; Perin, P.; Lucas, J.M.; Nelson, P.S.; Pöhlmann, S.; Soilleux, E.J. Influenza and SARS-Coronavirus Activating Proteases TMPRSS2 and HAT Are Expressed at Multiple Sites in Human Respiratory and Gastrointestinal Tracts. *PLoS ONE* **2012**, *7*, e35876. [CrossRef] [PubMed]

22. Simmons, G.; Zmora, P.; Gierer, S.; Heurich, A.; Pöhlmann, S. Proteolytic activation of the SARS-coronavirus spike protein: Cutting enzymes at the cutting edge of antiviral research. *Antivir. Res.* **2013**, *100*, 605–614. [CrossRef] [PubMed]

23. Mahoney, M.; Damalanka, V.C.; Tartell, M.A.; Chung, D.H.; Lourenço, A.L.; Pwee, D.; Mayer Bridwell, A.E.; Hoffmann, M.; Voss, J.; Karmakar, P.; et al. A novel class of TMPRSS2 inhibitors potently block SARS-CoV-2 and MERS-CoV viral entry and protect human epithelial lung cells. *Proc. Natl. Acad. Sci. USA* **2021**, *118*, e2108728118. [CrossRef] [PubMed]

24. Hoffmann, M.; Kleine-Weber, H.; Schroeder, S.; Krüger, N.; Herrler, T.; Erichsen, S.; Schiergens, T.S.; Herrler, G.; Wu, N.H.; Nitsche, A.; et al. SARS-CoV-2 Cell Entry Depends on ACE2 and TMPRSS2 and Is Blocked by a Clinically Proven Protease Inhibitor. *Cell* **2020**, *181*, 271–280.e8. [CrossRef]

25. Jackson, C.B.; Farzan, M.; Chen, B.; Choe, H. Mechanisms of SARS-CoV-2 entry into cells. *Nat. Rev. Mol. Cell Biol.* **2022**, *23*, 3–20. [CrossRef]

26. Zhao, M.M.; Yang, W.L.; Yang, F.Y.; Zhang, L.; Huang, W.J.; Hou, W.; Fan, C.F.; Jin, R.H.; Feng, Y.M.; Wang, Y.C.; et al. Cathepsin L plays a key role in SARS-CoV-2 infection in humans and humanized mice and is a promising target for new drug development. *Signal Transduct. Target. Ther.* **2021**, *6*, 134. [CrossRef]

27. Bestle, D.; Heindl, M.R.; Limburg, H.; Pilgram, O.; Moulton, H.; Stein, D.A.; Hardes, K.; Eickmann, M.; Dolnik, O.; Rohde, C.; et al. TMPRSS2 and furin are both essential for proteolytic activation of SARS-CoV-2 in human airway cells. *Life Sci. Alliance* **2020**, *3*, e1–e14. [CrossRef]

28. Li, F.; Han, M.; Dai, P.; Xu, W.; He, J.; Tao, X.; Wu, Y.; Tong, X.; Xia, X.; Guo, W.; et al. Distinct mechanisms for TMPRSS2 expression explain organ-specific inhibition of SARS-CoV-2 infection by enzalutamide. *Nat. Commun.* **2021**, *12*, 866. [CrossRef]

29. Wettstein, L.; Knaff, P.M.; Kersten, C.; Müller, P.; Weil, T.; Conzelmann, C.; Müller, J.A.; Brückner, M.; Hoffmann, M.; Pöhlmann, S.; et al. Peptidomimetic inhibitors of TMPRSS2 block SARS-CoV-2 infection in cell culture. *Commun. Biol.* **2022**, *5*, 681. [CrossRef]

30. Sanders, B.C.; Pokhrel, S.; Labbe, A.D.; Mathews, I.I.; Cooper, C.J.; Davidson, R.B.; Phillips, G.; Weiss, K.L.; Zhang, Q.; O'Neill, H.; et al. Potent and selective covalent inhibition of the papain-like protease from SARS-CoV-2. *Nat. Commun.* **2023**, *14*, 1733. [CrossRef]

31. Welker, A.; Kersten, C.; Müller, C.; Madhugiri, R.; Zimmer, C.; Müller, P.; Zimmermann, R.; Hammerschmidt, S.; Maus, H.; Ziebuhr, J.; et al. Structure-Activity Relationships of Benzamides and Isoindolines Designed as SARS-CoV Protease Inhibitors Effective against SARS-CoV-2. *ChemMedChem* **2021**, *16*, 340–354. [CrossRef]

32. Kincaid, J.R.; Caravez, J.C.; Iyer, K.S.; Kavthe, R.D.; Fleck, N.; Aue, D.H.; Lipshutz, B.H. A sustainable synthesis of the SARS-CoV-2 Mpro inhibitor nirmatrelvir, the active ingredient in Paxlovid. *Commun. Chem.* **2022**, *5*, 156. [CrossRef]

33. Joossens, J.; Ali, O.M.; El-Sayed, I.; Surpateanu, G.; Van der Veken, P.; Lambeir, A.-M.; Setyono-Han, B.; Foekens, J.A.; Schneider, A.; Schmalix, W.; et al. Small, Potent, and Selective Diaryl Phosphonate Inhibitors for Urokinase-Type Plasminogen Activator with In Vivo Antimetastatic Properties. *J. Med. Chem.* **2007**, *50*, 6638–6646. [CrossRef]

34. Zeslawska, E.; Jacob, U.; Schweinitz, A.; Coombs, G.; Bode, W.; Madison, E. Crystals of Urokinase Type Plasminogen Activator Complexes Reveal the Binding Mode of Peptidomimetic Inhibitors. *J. Mol. Biol.* **2003**, *328*, 109–118. [CrossRef]

35. Lonsdale, R.; Ward, R.A. Structure-based design of targeted covalent inhibitors. *Chem. Soc. Rev.* **2018**, *47*, 3816–3830. [CrossRef]

36. Baillie, T.A. Targeted Covalent Inhibitors for Drug Design. *Angew. Chem. Int. Ed.* **2016**, *55*, 13408–13421. [CrossRef]

37. De Cesco, S.; Kurian, J.; Dufresne, C.; Mittermaier, A.K.; Moitessier, N. Covalent inhibitors design and discovery. *Eur. J. Med. Chem.* **2017**, *138*, 96–114. [CrossRef]

38. Sun, G.; Sui, Y.; Zhou, Y.; Ya, J.; Yuan, C.; Jiang, L.; Huang, M. Structural Basis of Covalent Inhibitory Mechanism of TMPRSS2-Related Serine Proteases by Camostat. *J. Virol.* **2021**, *95*, 10–1128. [CrossRef]

39. Müller, P.; Meta, M.; Meidner, J.L.; Schwickert, M.; Meyr, J.; Schwickert, K.; Kersten, C.; Zimmer, C.; Hammerschmidt, S.J.; Frey, A.; et al. Investigation of the Compatibility between Warheads and Peptidomimetic Sequences of Protease Inhibitors—A Comprehensive Reactivity and Selectivity Study. *Int. J. Mol. Sci.* **2023**, *24*, 7226. [CrossRef]

40. Kwon, H.; Ha, H.; Jeon, H.; Jang, J.; Son, S.-H.; Lee, K.; Park, S.-K.; Byun, Y. Structure-activity relationship studies of dipeptide-based hepsin inhibitors with Arg bioisosteres. *Bioorg. Chem.* **2021**, *107*, 104521. [CrossRef]

41. Hoffmann, M.; Hofmann-Winkler, H.; Smith, J.C.; Krüger, N.; Arora, P.; Sørensen, L.K.; Søgaard, O.S.; Hasselstrøm, J.B.; Winkler, M.; Hempel, T.; et al. Camostat mesylate inhibits SARS-CoV-2 activation by TMPRSS2-related proteases and its metabolite GBPA exerts antiviral activity. *EBioMedicine* **2021**, *65*, 103255. [CrossRef] [PubMed]

42. Han, Z.; Harris, P.K.; Karmakar, P.; Kim, T.; Owusu, B.Y.; Wildman, S.A.; Klampfer, L.; Janetka, J.W. α-Ketobenzothiazole Serine Protease Inhibitors of Aberrant HGF/c-MET and MSP/RON Kinase Pathway Signaling in Cancer. *ChemMedChem* **2016**, *11*, 585–599. [CrossRef] [PubMed]

43. Ludewig, S.; Kossner, M.; Schiller, M.; Baumann, K.; Schirmeister, T. Enzyme Kinetics and Hit Validation in Fluorimetric Protease Assays. *Curr. Top. Med. Chem.* **2010**, *10*, 368–382. [CrossRef] [PubMed]

44. Li, C.Y.; de Veer, S.J.; Law, R.H.P.; Whisstock, J.C.; Craik, D.J.; Swedberg, J.E. Characterising the Subsite Specificity of Urokinase-Type Plasminogen Activator and Tissue-Type Plasminogen Activator using a Sequence-Defined Peptide Aldehyde Library. *ChemBioChem* **2019**, *20*, 46–50. [CrossRef] [PubMed]

45. Green, K.A.; Lund, L.R. ECM degrading proteases and tissue remodelling in the mammary gland. *BioEssays* **2005**, *27*, 894–903. [CrossRef] [PubMed]

46. Ortiz-Zapater, E.; Peiró, S.; Roda, O.; Corominas, J.M.; Aguilar, S.; Ampurdanés, C.; Real, F.X.; Navarro, P. Tissue Plasminogen Activator Induces Pancreatic Cancer Cell Proliferation by a Non-Catalytic Mechanism That Requires Extracellular Signal-Regulated Kinase 1/2 Activation through Epidermal Growth Factor Receptor and Annexin A2. *Am. J. Pathol.* **2007**, *170*, 1573–1584. [CrossRef] [PubMed]

47. Tanaka, K.A.; Key, N.S.; Levy, J.H. Blood Coagulation: Hemostasis and Thrombin Regulation. *Anesth. Analg.* **2009**, *108*, 1433–1446. [CrossRef]

48. Borensztajn, K.; Spek, C.A. Blood coagulation factor Xa as an emerging drug target. *Expert Opin. Ther. Targets* **2011**, *15*, 341–349. [CrossRef]

49. List, K.; Bugge, T.H.; Szabo, R. Matriptase: Potent Proteolysis on the Cell Surface. *Mol. Med.* **2006**, *12*, 1–7. [CrossRef]

50. Gustafsson, D.; Nyström, J.E.; Carlsson, S.; Bredberg, U.; Eriksson, U.; Gyzander, E.; Elg, M.; Antonsson, T.; Hoffmann, K.J.; Ungell, A.L.; et al. The Direct Thrombin Inhibitor Melagatran and Its Oral Prodrug H 376/95: Intestinal Absorption Properties, Biochemical and Pharmacodynamic Effects. *Thromb. Res.* **2001**, *101*, 171–181. [CrossRef]

51. Sibinovska, N.; Žakelj, S.; Trontelj, J.; Kristan, K. Applicability of RPMI 2650 and Calu-3 Cell Models for Evaluation of Nasal Formulations. *Pharmaceutics* **2022**, *14*, 369. [CrossRef]

52. Elezović, A.; Marić, A.; Biščević, A.; Hadžiabdić, J.; Škrbo, S.; Špirtović-Halilović, S.; Rahić, O.; Vranić, E.; Elezović, A. In vitro pH dependent passive transport of ketoprofen and metformin. *ADMET DMPK* **2020**, *9*, 57–68. [CrossRef]

53. Butnarasu, C.; Caron, G.; Pacheco, D.P.; Petrini, P.; Visentin, S. Cystic Fibrosis Mucus Model to Design More Efficient Drug Therapies. *Mol. Pharm.* **2022**, *19*, 520–531. [CrossRef]

54. Hauel, N.H.; Nar, H.; Priepke, H.; Ries, U.; Stassen, J.-M.; Wienen, W. Structure-Based Design of Novel Potent Nonpeptide Thrombin Inhibitors. *J. Med. Chem.* **2002**, *45*, 1757–1766. [CrossRef]

55. Schade, D.; Kotthaus, J.; Riebling, L.; Kotthaus, J.; Müller-Fielitz, H.; Raasch, W.; Hoffmann, A.; Schmidtke, M.; Clement, B. Zanamivir Amidoxime- and N-Hydroxyguanidine-Based Prodrug Approaches to Tackle Poor Oral Bioavailability. *J. Pharm. Sci.* **2015**, *104*, 3208–3219. [CrossRef]

56. Dave, V.S.; Gupta, D.; Yu, M.; Nguyen, P.; Varghese Gupta, S. Current and evolving approaches for improving the oral permeability of BCS Class III or analogous molecules. *Drug Dev. Ind. Pharm.* **2017**, *43*, 177–189. [CrossRef]

57. Fuchs, N.; Meta, M.; Schuppan, D.; Nuhn, L.; Schirmeister, T. Novel Opportunities for Cathepsin S Inhibitors in Cancer Immunotherapy by Nanocarrier-Mediated Delivery. *Cells* **2020**, *9*, 2021. [CrossRef]

58. Lee, J.; Choi, M.-K.; Song, I.-S. Recent Advances in Doxorubicin Formulation to Enhance Pharmacokinetics and Tumor Targeting. *Pharmaceuticals* **2023**, *16*, 802. [CrossRef]

59. Kansy, M.; Senner, F.; Gubernator, K. Physicochemical High Throughput Screening: Parallel Artificial Membrane Permeation Assay in the Description of Passive Absorption Processes. *J. Med. Chem.* **1998**, *41*, 1007–1010. [CrossRef]

60. St-Georges, C.; Désilets, A.; Béliveau, F.; Ghinet, M.; Dion, S.P.; Colombo, É.; Boudreault, P.-L.; Najmanovich, R.J.; Leduc, R.; Marsault, É. Modulating the selectivity of matriptase-2 inhibitors with unnatural amino acids. *Eur. J. Med. Chem.* **2017**, *129*, 110–123. [CrossRef]

61. Costanzo, M.J.; Yabut, S.C.; Almond, H.R.; Andrade-Gordon, P.; Corcoran, T.W.; de Garavilla, L.; Kauffman, J.A.; Abraham, W.M.; Recacha, R.; Chattopadhyay, D.; et al. Potent, Small-Molecule Inhibitors of Human Mast Cell Tryptase. Antiasthmatic Action of a Dipeptide-Based Transition-State Analogue Containing a Benzothiazole Ketone. *J. Med. Chem.* **2003**, *46*, 3865–3876. [CrossRef]

62. Furlan, A.; Colombo, F.; Kover, A.; Issaly, N.; Tintori, C.; Angeli, L.; Leroux, V.; Letard, S.; Amat, M.; Asses, Y.; et al. Identification of new aminoacid amides containing the imidazo[2,1-b]benzothiazol-2-ylphenyl moiety as inhibitors of tumorigenesis by oncogenic Met signaling. *Eur. J. Med. Chem.* **2012**, *47*, 239–254. [CrossRef]

63. Capaldo, L.; Quadri, L.L.; Merli, D.; Ravelli, D. Photoelectrochemical cross-dehydrogenative coupling of benzothiazoles with strong aliphatic C–H bonds. *Chem. Commun.* **2021**, *57*, 4424–4427. [CrossRef]

64. Kerns, E.H.; Di, L.; Petusky, S.; Farris, M.; Ley, R.; Jupp, P. Combined Application of Parallel Artificial Membrane Permeability Assay and Caco-2 Permeability Assays in Drug Discovery. *J. Pharm. Sci.* **2004**, *93*, 1440–1453. [CrossRef]

65. Avdeef, A. *Absorption and Drug Development*; Wiley: Hoboken, NJ, USA, 2003. [CrossRef]

66. Sugano, K.; Hamada, H.; Machida, M.; Ushio, H. High Throughput Prediction of Oral Absorption: Improvement of the Composition of the Lipid Solution Used in Parallel Artificial Membrane Permeation Assay. *SLAS Discov.* **2001**, *6*, 189–196. [CrossRef]

67. Hammerschmidt, S.J.; Maus, H.; Weldert, A.C.; Gütschow, M.; Kersten, C. Improving binding entropy by higher ligand symmetry?—A case study with human matriptase. *RSC Med. Chem.* **2023**, *14*, 969–982. [CrossRef]

68. Ehnebom, J.; Pusa, S.; Björquist, P.; Deinum, J. Comparison of chromogenic substrates for tissue plasminogen activator and the effects on the stability of plasminogen activator inhibitor type-1. *Fibrinolysis Proteolysis* **1997**, *11*, 287–293. [CrossRef]

69. Tapp, H.J.; Grundmann, C.; Kusch, M.; Konig, H. Calibrating Thrombin Generation in Different Samples: Less Effort with a Less Efficient Substrate. *Open Atheroscler. Thromb. J.* **2009**, *2*, 6–11. [CrossRef]

70. Edwards, S.T.; Betz, A.; James, H.L.; Thompson, E.; Yonkovich, S.J.; Sinha, U. Differences between human and rabbit coagulation factor X—Implications for in vivo models of thrombosis. *Thromb. Res.* **2002**, *106*, 71–79. [CrossRef]

71. Wilkinson, D.J.; Habgood, A.; Lamb, H.K.; Thompson, P.; Hawkins, A.R.; Désilets, A.; Leduc, R.; Steinmetzer, T.; Hammami, M.; Lee, M.S.; et al. Matriptase Induction of Metalloproteinase-Dependent Aggrecanolysis In Vitro and In Vivo: Promotion of Osteoarthritic Cartilage Damage by Multiple Mechanisms. *Arthritis Rheumatol.* **2017**, *69*, 1601–1611. [CrossRef]

72. Steinmetzer, T.; Schweinitz, A.; Stürzebecher, A.; Dönnecke, D.; Uhland, K.; Schuster, O.; Steinmetzer, P.; Müller, F.; Friedrich, R.; Than, M.E.; et al. Secondary Amides of Sulfonylated 3-Amidinophenylalanine. New Potent and Selective Inhibitors of Matriptase. *J. Med. Chem.* **2006**, *49*, 4116–4126. [CrossRef]